The hydrodynamics of thin floating plates

Christopher J. Damaren [*]

University of Toronto, Institute for Aerospace Studies, 4925 Dufferin Street, Toronto, Ontario, M3H 5T6, Canada

Abstract

The radiation and diffraction problems are considered in the frequency domain for a thin elastic plate of rectangular planform floating in an irrotational, incompressible ocean of infinite depth. The inner potential field inside a hemisphere surrounding the plate is represented using a spherical harmonic expansion which suits the geometry and zero-draft nature of the plate. Problems associated with distributing sources in the free surface are avoided. The Chen and Mei variational principle is used to weakly match this inner solution and its normal derivative to an outer field described by distributing sources on the exterior of the hemisphere. The validity of the procedure is first illustrated by considering a heaving circular disk. Numerous hydrodynamic coefficients are presented as benchmark data for floating flexible structures. The transient motion of the plate is simulated using rational approximations (in the frequency domain) to the radiation impedance and diffraction mapping which are implemented as ODE's in the time domain. © 2001 Elsevier Science Ltd. All rights reserved.

1. Introduction

The frequency domain analysis of floating bodies within the context of linearized free-surface hydrodynamics has been well established for some time (Wehausen, 1971) and the underlying boundary value problem is well known for both the radiation and diffraction cases. Numerical and analytical studies of the added mass and damping coefficients and the complex diffraction force coefficients have been pub-

* Tel.: +1-416-667-7704; fax: +1-416-667-7799.
  E-mail address: cjd@sdr.utias.utoronto.ca (C.J. Damaren).

lished for an extensive set of rigid bodies exhibiting a subset of the six possible fundamental motions.

Although the underlying approach to floating rigid bodies is readily extended to structurally flexible bodies by extending the number of fundamental motions (as noted by Newman, 1994, for example), there have been few published results in this situation. Simple beam and plate models can serve as suitable benchmark problems in this context. This paper concentrates on the hydrodynamics of thin floating rectangular plates. In addition to exhibiting simple, but analytically unavailable, vibration modes with well-defined symmetries, such models have been advocated as a logical starting point in the analysis and design of floating airports. Wu et al. (1995) have analyzed a two-dimensional version of the problem by assuming the plate to have a very large aspect ratio. The finite-depth nature of the fluid allowed an eigenfunction expansion-matching method to be used which patched various series expansions for the (radiation and diffraction) potential along finite vertical interfaces.

Thin elastic floating plates are representative of so-called dock problems where the entire structure is located in the undisturbed free surface and wetted on only one side. Integral equation techniques employing three-dimensional source distributions can be problematical when applied to dock problems. Buchner (1993) reviewed the zero-draft limit of the three-dimensional Green's function and its use in shallow draft problems. A major conclusion was the limited applicability of the theory with good approximations to the hydrodynamic coefficients typically occuring only at very low frequencies. Notwithstanding these conclusions, the zero-draft form of the integral equations was used by Meylan (1997) to formulate the radiation problem for a thin floating plate.

In this paper, a complete study is made of the frequency-domain hydrodynamics for a thin floating plate. A novel use of the Chen and Mei (1974) and Mei (1989) variational principle is used to determine the radiation and diffraction fields for several rigid and elastic modes. The inner field within a hemisphere encompassing the plate is described using a spherical harmonic expansion which ideally suits the geometry given the zero-draft nature of the plate. In addition, it avoids the problems inherent in having sources lie in the free surface. The outer field is described by distributed sources on the exterior of the hemisphere and it along with its normal derivative are matched to those of the inner field using the variational principle.

The validity of our approach is established by first applying it to the heaving motions of a rigid circular disk and comparing the added mass and damping coefficients with those previously published by Miles (1987) and Martin and Farina (1997). For comparison, a zero-draft panel method is also used to expose the flaws inherent in distributing sources in the free surface.

Lastly, transient time-domain solutions for the motions of the plate in response to a transient incident wave field and a moving point load are presented. These employ the procedures of Damaren (1999) to determine rational approximations of the radiation impedance and diffraction mapping in the frequency (Laplace transform) domain. These can then be implemented in the time domain as nonhomogeneous, constant–coefficient, ordinary differential equations forced by the body velocities and incident wave height, respectively.

2. The boundary value problem

The motion equation for a thin floating plate lying in the free surface is given by

$$\sigma(\mathbf{r})\ddot{w}+D\nabla^4w(\mathbf{r},t)=p(x,y,t) \tag{1}$$

where $p(x,y,t)$ is the hydrodynamic pressure, $w(x,y,t)$ is the deflection of the plate, D is the constant modulus of rigidity, and σ is the constant mass density per unit area. In addition, there are boundary conditions on the plate edges which state that they are free of force and moment. We use a coordinate system $\mathbf{r}=[xyz]^T$ in which the x–y plane coincides with the mean free surface and the z-axis is vertically upwards. The plate is assumed to be rectangular with dimensions $a{\times}b$ and corresponding area A and wetted surface B.

It is well known that Eq. (1) can be reformulated as a variational problem which forms the basis for spatial discretization. Here, we take

$$w(x,y,t)=\sum_{\alpha=1}^{N}\psi_\alpha(x,y)q_\alpha(t)=\mathbf{\Psi}(\mathbf{r})\mathbf{q}(t) \tag{2}$$

where $\mathbf{\Psi}=\text{row}\{\psi_\alpha\}$ and $\mathbf{q}=\text{col}\{q_\alpha\}$. For a rectangular plate, we take $\psi_1=1$, $\psi_2=x$, $\psi_3=y$, …, corresponding to an n_x by n_y array of Legendre polynomials in x and y: $\psi_\alpha=P_n(x)\,P_m(y)$, $n,m=0,1,2,…$. The ensuing discrete motion equations are of the standard form

$$\mathbf{M}\ddot{\mathbf{q}}+\mathbf{K}\mathbf{q}=\int_B\mathbf{\Psi}^Tp(x,y,t)dA \tag{3}$$

where $M_{\alpha\beta}=\int_B\psi_\alpha\psi_\beta\sigma dA$ and

$$K_{\alpha\beta}=D\int\int_B\left[\frac{\partial^2\psi_\alpha}{\partial x^2}\frac{\partial^2\psi_\beta}{\partial x^2}+\frac{\partial^2\psi_\alpha}{\partial y^2}\frac{\partial^2\psi_\beta}{\partial y^2}+v\frac{\partial^2\psi_\alpha}{\partial x^2}\frac{\partial^2\psi_\beta}{\partial y^2}+v\frac{\partial^2\psi_\beta}{\partial x^2}\frac{\partial^2\psi_\alpha}{\partial y^2}+2(1\right.$$

$$\left.-v)\frac{\partial^2\psi_\alpha}{\partial x\partial y}\frac{\partial^2\psi_\beta}{\partial x\partial y}\right]dxdy.$$

Letting $\mathbf{q}(t)=\text{Re}\{\bar{\mathbf{q}}_\alpha\exp(j\Omega_\alpha t)\}$ in the homogeneous form of Eq. (3) leads to the eigenproblem $\Omega_\alpha^2\,\mathbf{M}\bar{\mathbf{q}}_\alpha=\mathbf{K}\bar{\mathbf{q}}_\alpha$, $\alpha=1…N$, which permits the determination of the vibration frequencies Ω_α and the corresponding eigenvectors $\bar{\mathbf{q}}_\alpha$ with corresponding mode shapes $w_\alpha(x,y)=\mathbf{\Psi}(x,y)\,\bar{\mathbf{q}}_\alpha$. A modal expansion of the form $w(x,y,t)=\Sigma_\alpha w_\alpha(x,y)\,\eta_\alpha(t)$ leads to uncoupled motion equations of the form

$$\ddot{\eta}_\alpha+\Omega_\alpha^2\eta_\alpha(t)=f_\alpha(t)=\int_B w_\alpha p(x,y,t)dA \tag{4}$$

assuming that $\mathbf{q}_\alpha^T \mathbf{M} \mathbf{q}_\beta = \delta_{\alpha\beta}$.

The motion of the fluid is governed by the velocity potential $\Phi(\mathbf{r},t)$ which, in $V=\{z \leq 0 \backslash B\}$ satisfies

$$\nabla^2 \Phi = 0, \mathbf{r} \in V; \quad \frac{\partial^2 \Phi}{\partial t^2} = -g\frac{\partial \Phi}{\partial z}, \mathbf{r} \in F; \tag{5}$$

$$\lim_{z \to -\infty} \frac{\partial \Phi}{\partial z} = 0; \quad \frac{\partial \Phi}{\partial n} = -\frac{\partial \Phi}{\partial z} = \sum_{\alpha=1}^{N} w_\alpha(\mathbf{r})\dot{\eta}_\alpha, \mathbf{r} \in B. \tag{6}$$

(n will indicate the direction of the outward normal to the body surface B, i.e., into the fluid). Here F denotes the free surface and g is the acceleration due to gravity. We make the standard decomposition

$$\Phi = \Phi_I + \Phi_S + \Phi_R \tag{7}$$

where Φ_I describes the incident wave field, Φ_S is the scattered field, and Φ_R is the radiated field.

For simplicity, the incident wave field is assumed to consist of a transient system corresponding to a superposition of waves propagating in the x-direction, i.e.,

$$\Phi_I(\mathbf{r},t) = \frac{1}{2\pi}\int_{-\infty}^{\infty} \tilde{\phi}_I(j\omega)\tilde{\zeta}_0(j\omega)e^{j\omega t}d\omega \tag{8}$$

where

$$\tilde{\phi}_I = \frac{jg}{\omega}e^{kz - jk'x}, \quad k = \omega^2/g, \quad k' = k \, sgn(\omega). \tag{9}$$

The potential in Eq. (9) when multiplied by $e^{j\omega t}$ is recognized as that corresponding to a plane progressing wave in the positive x-direction with time dependence of this form.

It is important to realize that the Fourier transform of the transient problem, $F\{\Phi_I(\mathbf{r},t)\} \triangleq \tilde{\Phi}_I(\mathbf{r},j\omega)$, produces a formulation that is equivalent to an assumed time-harmonic dependence of the form $\Phi_I(\mathbf{r},t) = \tilde{\phi}_I(j\omega)\tilde{\zeta}_0(j\omega)\exp(j\omega t)$. It is more amenable to a later recovery of solutions of the transient problem. It is readily verified that the height of the free surface is given by

$$\zeta_I(x,y,t) = -\frac{1}{g}\frac{\partial \Phi_I}{\partial t}\Big|_{z=0} = \frac{1}{2\pi}\int_{-\infty}^{\infty} \tilde{\zeta}_0(j\omega)e^{-jk'x}e^{j\omega t}d\omega \tag{10}$$

which yields $\zeta_0(t) \triangleq \zeta_I(0,0,t) = F^{-1}\{\tilde{\zeta}_0(j\omega)\}$ upon setting $x=0$. Therefore, ζ_0 is the reference wave height at the datum $r=0$. Using the properties of the Fourier transform, Eq. (8) implies that

$$\Phi_I(\mathbf{r},t) = F^{-1}\{\tilde{\phi}_I(j\omega)\tilde{\zeta}_0(j\omega)\} = \phi_I(\mathbf{r},t) * \zeta_0(t) \tag{11}$$

where $*$ denotes temporal convolution. Therefore $\Phi_I(\mathbf{r},t)=\phi_I(\mathbf{r},t)$ when $\zeta_0(t)=\delta(t)$.

In a similar manner, the scattered and radiated fields are further decomposed into

$$\Phi_S=\phi_S*\zeta_0(t), \; \Phi_R=\sum_{\alpha=1}^{N}\phi_\alpha*\dot{q}_\alpha \tag{12}$$

where

$$\frac{\partial\phi_S}{\partial z}=-\frac{\partial\phi_I}{\partial z}, \; \frac{\partial\phi_\alpha}{\partial z}=-n_\alpha\delta(t), \; (x,y)\in B \tag{13}$$

with $n_\alpha=-w_\alpha(x,y)$. In addition, ϕ_S and ϕ_α are bounded as are their first derivatives as $R\rightarrow\infty$ (R is the spherical radius). The frequency domain potentials $\tilde{\phi}_s$ and $\tilde{\phi}_\alpha$ satisfy the equations produced by Fourier transforming Eqs. (5)–(13). In particular, the free-surface boundary condition becomes $\partial\tilde{\phi}_\alpha/\partial z=k\;\tilde{\phi}_\alpha$. In addition, they satisfy an outgoing radiation condition as $r\triangleq\sqrt{x^2+y^2}\rightarrow\infty$.

Using Bernoulli's equation, the fluid pressure is given by

$$p(x,y,t)=-\rho\frac{\partial\Phi}{\partial t}-\rho gz \tag{14}$$

where ρ is the fluid density. Working in the frequency domain and using the Fourier transforms of Eqs. (4), (14), (7), (11) and (12) the total force in mode α is

$$\tilde{f}_\alpha(j\omega)=-\sum_{\beta=1}^{N}K_{s,\alpha\beta}\tilde{\eta}_\alpha(j\omega)+\tilde{f}_{D\alpha}(j\omega)+\tilde{f}_{R\alpha}(j\omega) \tag{15}$$

where the entries of the hydrostatic restoring matrix are shown by Newman (1994) to be given by

$$K_{s,\alpha\beta}=\rho g\int_B w_\alpha w_\beta dA=(\rho g/\sigma)\delta_{\alpha\beta}.$$

The diffraction and radiation forces satisfy

$$\tilde{f}_{D\alpha}(j\omega)=\tilde{H}_{D\alpha}(j\omega)\tilde{\zeta}_0(j\omega) \tag{16}$$

$$\tilde{f}_{R\alpha}(j\omega)=-\sum_{\beta=1}^{N}\tilde{H}_{R\alpha\beta}(j\omega)[j\omega\tilde{\eta}_\beta(j\omega)] \tag{17}$$

with

$$\tilde{H}_{D\alpha}(j\omega)=j\omega\rho\int_B[\tilde{\phi}_I+\tilde{\phi}_S]n_\alpha dA, \tag{18}$$

$$\tilde{H}_{R,\alpha\beta}(j\omega)=j\omega\rho\int_B[\tilde{\phi}_\beta n_\alpha]dA=j\omega\mu_{\alpha\beta}+\lambda_{\alpha\beta} \tag{19}$$

$\lambda_{\alpha\beta}=Re\{\tilde{H}_{R,\alpha\beta}(j\omega)\}$ are the added damping coefficients, and $\mu_{\alpha\beta}=\omega^{-1}\ Im\{\tilde{H}_{R,\alpha\beta}(j\omega)\}$ are the added mass coeffients.

The Laplace transform is also used here with $\tilde{\zeta}_0(s)=L\{\zeta_0(t)\}$. In the absence of arguments, say $\tilde{\zeta}_0$, the Fourier transform is intended. The s-domain formulation of the problem is illustrated in Fig. 1. The major contribution of the paper lies in the accurate determination of $\tilde{H}_{D\alpha}(j\omega)$ and $\tilde{H}_{R,\alpha\beta}(j\omega)$ at many frequencies. However, the curve-fitting techniques of Damaren (1999) will be employed which fit this data with rational functions of s, $\tilde{H}_{D\alpha}(s)$ and $\tilde{H}_{R,\alpha\beta}(s)$. This permits the diffraction mapping and the radiation impedance to be realized in the time domain as systems of non-homogeneous constant–coefficient ordinary differential equations. By combining them with Eq. (4), a similar description is then available for the mapping from $\zeta_0(t)$ to $w(x,y,t)$.

3. Solution by integral equations

It is well known that the solutions of the hydrodynamic boundary value problems, say $\tilde{\phi}=\tilde{\phi}_\alpha$ or $\tilde{\phi}=\tilde{\phi}_s$, can be obtained in terms of a distribution of sources $\gamma(x,y)$,

$$\tilde{\phi}(\mathbf{r})=\int_B G(\mathbf{r},\boldsymbol{\xi})\gamma(\boldsymbol{\xi})dA_\xi, \tag{20}$$

where the source density γ is a solution to a Fredholm integral equation of the form

$$-2\pi\gamma(\mathbf{r})+\int_B\frac{\partial G(\mathbf{r},\boldsymbol{\xi})}{\partial n_r}\gamma(\boldsymbol{\xi})dA_\xi=\frac{\partial\tilde{\phi}(\mathbf{r})}{\partial n_r} \tag{21}$$

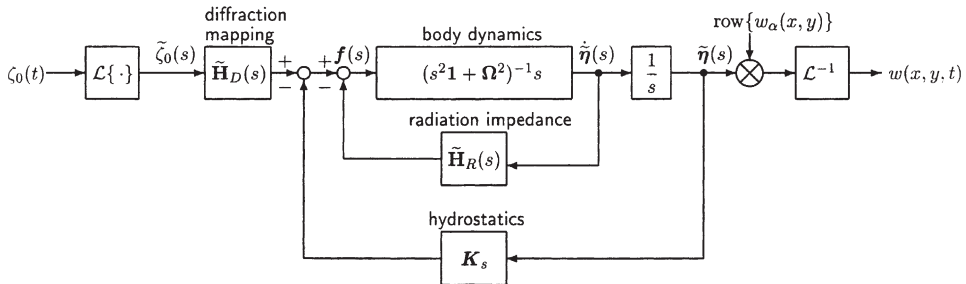Fig. 1.   Block diagram of combined hydroelastic problem.

and $G(\mathbf{r},\boldsymbol{\xi})$ is the Green's function which satisfies Laplace's equation and the free surface, bottom, and radiation conditions:

$$G(\mathbf{r},\boldsymbol{\xi})=\frac{1}{R_\xi}+\frac{1}{R_1}-ke^{-Y}[\pi(Y_0(X)+\mathbf{H}_0(X))+2\int\limits_0^Y e^t(X^2+t^2)^{-1/2}dt] \tag{22}$$

$$-2\pi jke^{-Y}J_0(X)$$

where

$$r_\xi=\sqrt{(x{-}\xi)^2+(y{-}\eta)^2}$$

$$R_\xi^2=r_\xi^2+(z{-}\zeta)^2,\ R_1^2=r_\xi^2+(z{+}\zeta)^2,$$

$$X=kr_\xi,\ Y=-k(z{+}\zeta),$$

$J_0(X)$ and $Y_0(X)$ are Bessel functions of the first and second kind, and $\mathbf{H}_0(X)$ is the Struve function. In this work, $G(\mathbf{r},\boldsymbol{\xi})$ and its normal derivative are calculated using the algorithms of Newman (1984).

The limiting case where $z=\zeta=0$ corresponding to a zero-draft structure has been discussed by several authors and is summarized by Buchner (1993). In this case, the integral in Eq. (22) vanishes and the Green's function becomes

$$G(\mathbf{r},\boldsymbol{\xi})=\frac{2}{R_\xi}-\pi k[Y_0(X)+\mathbf{H}_0(X)]-2\pi jkJ_0(X). \tag{23}$$

As $|\mathbf{r}{-}\boldsymbol{\xi}|{\to}0$, $G(\mathbf{r},\boldsymbol{\xi}){\to}2/R_\xi$ so that the factor of 2π in Eq. (21) is replaced by 4π and the "self panel effect" involved in implementing Eq. (20) (the calculation of $\int G(\mathbf{r},\boldsymbol{\xi})dA$ as $\mathbf{r}{\to}\boldsymbol{\xi}$) is multiplied by two. This shallow draft version of the integral equation formulation was adopted by Meylan (1997) in his study of floating plates and has the advantage of avoiding problems with irregular frequencies. However, as will now be shown, it appears to give correct results only in the low frequency limit.

3.1. Example — the heaving disc

Consider a thin disc with radius a which heaves in a harmonic fashion. This is a useful problem to consider because the low- and high-frequency asymptotics for the added mass and damping coefficients are known. According to Miles (1987), $\hat{\mu}\,(0)=8/3$ and $\hat{\mu}\,(\infty)=4/3$ where

$$\hat{\mu}=\mu/(\rho a^3),\ \ \hat{\lambda}=\lambda/(\omega\rho a^3).$$

The damping coefficients behave as $\hat{\lambda}=\pi^2\,ka/2$ as $ka{\to}0$, and $\hat{\lambda}{\to}8/(ka)$ as $ka{\to}\infty$.

The results obtained using the zero-draft panel method are given in Fig. 2 for an array of 40×12 sector-shaped flat panels with equal spacing in the circumferential and radial directions. Clearly, the asymptotic behavior of the added mass and damping coefficients is incorrect. (The curves labeled "variational" will be discussed in Section 4.)

The coefficients have been previously studied by Miles (1987) using a "variational interpolation" procedure applied to the integral equation describing $\tilde{\phi}_\alpha$. The zero-draft panel method exhibits reasonable agreement with those results for $ka \leq 1$ but the discrepancy grows substantially thereafter. It should be noted that the results of Miles are in agreement with those of Martin and Farina (1997) who discussed the difficulties in using the integral equation method for dock problems.

4. Variational formulation

Given the difficulty of accurately solving the problem by distributing sources on the plate, we use an alternative methodology which seeks to match a solution in an inner region containing the plate with an outer solution which satisfies the radiation condition. Let S denote the surface of a hemisphere of radius a_h that encloses the plate and is centred at the origin. Let V denote the interior of S and F denote the circular free surface inside the hemisphere less the plate surface B. The exterior of S in $z \leq 0$ is denoted by $\bar{V}$ and the corresponding free surface is $\bar{F}$. It is assumed to be bounded by a cylinder S_∞ whose radius tends to infinity and whose bottom B_∞ tends towards infinite depth. The spatial decomposition is illustrated in Fig. 3.

4.1. Radiation problem

For the radiation problem, we seek a solution for $\tilde{\phi}_\alpha$ in V which satisfies (i)$\nabla^2 \tilde{\phi}_\alpha = 0$ in V, (ii) $\partial \tilde{\phi}_\alpha / \partial z = k \tilde{\phi}_\alpha$ on F, and (iii) $\partial \tilde{\phi}_\alpha / \partial z = w_\alpha$ on B. In the exterior region, we seek a solution $\bar{\phi}_\alpha$ which satisfies Laplace's equation, the free surface condition on $\bar{F}$, the bottom condition on B_∞, and the radiation condition on S_∞. In addition, the matching conditions

$$\tilde{\phi}_\alpha(\mathbf{r},j\omega)=\bar{\phi}_\alpha(\mathbf{r},j\omega), \ \frac{\partial \tilde{\phi}_\alpha}{\partial n}(\mathbf{r},j\omega)=\frac{\partial \bar{\phi}_\alpha}{\partial n}(\mathbf{r},j\omega), \ \mathbf{r} \in S \tag{24}$$

should hold on the hemisphere, where n is the outward (from the hemisphere) normal. (For the duration of this section the $j\omega$ dependence is neglected for clarity.)

The variational principle of Chen and Mei (1974) and Mei (1989) provides an elegant solution to the problem. They have shown that minimization of the functional

$$J(\tilde{\phi}_\alpha,\bar{\phi}_\alpha)=\frac{1}{2}\int_V \nabla\tilde{\phi}_\alpha\cdot\nabla\tilde{\phi}_\alpha dV-\frac{1}{2}k\int_F \tilde{\phi}_\alpha^2 dS+\int_B \tilde{\phi}_\alpha n_\alpha dA+\int_S\left(\frac{1}{2}\bar{\phi}_\alpha-\tilde{\phi}_\alpha\right)\frac{\partial\bar{\phi}_\alpha}{\partial n}dS \tag{25}$$

yields a function $\tilde{\phi}_\alpha$ which satisfies (i), above, weakly with (ii), (iii), and the matching
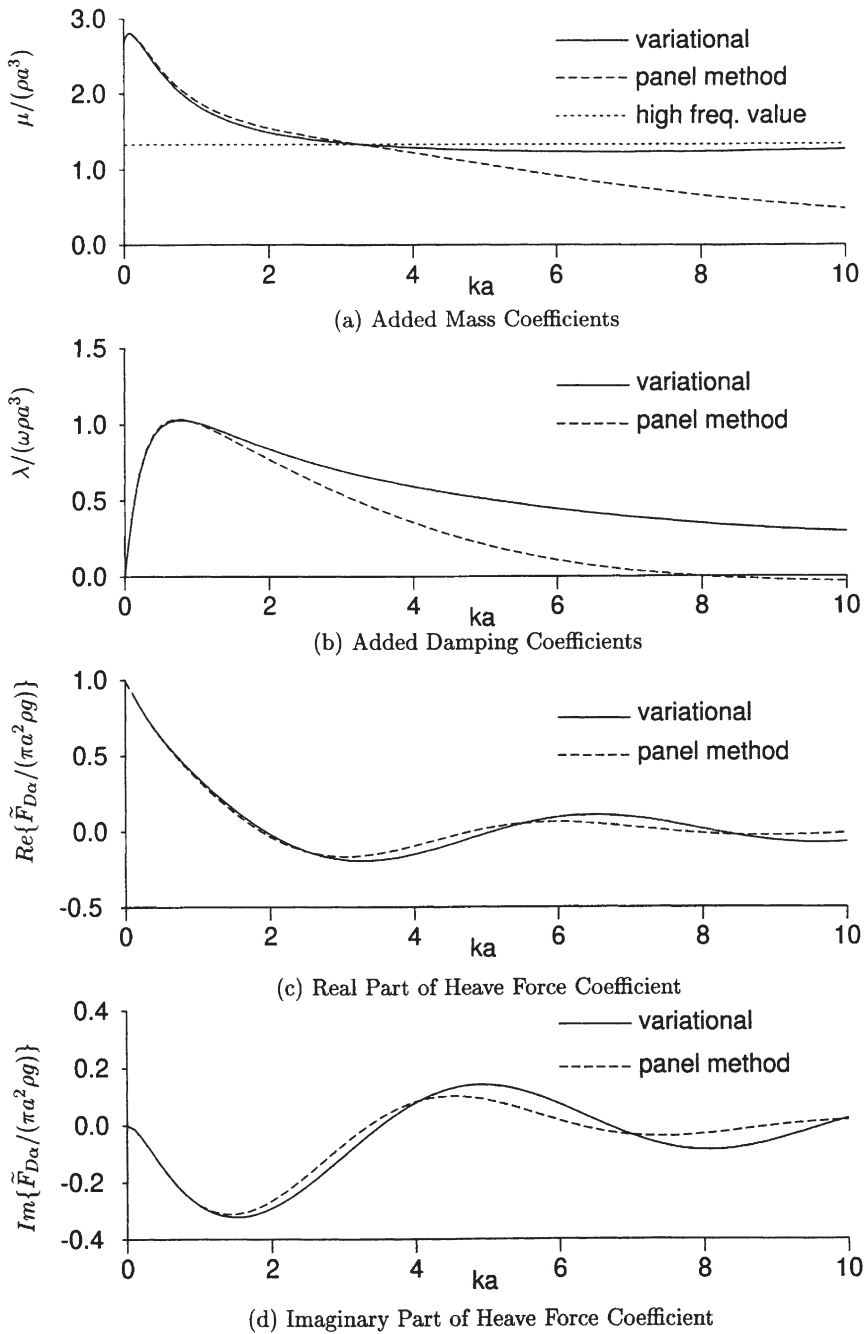
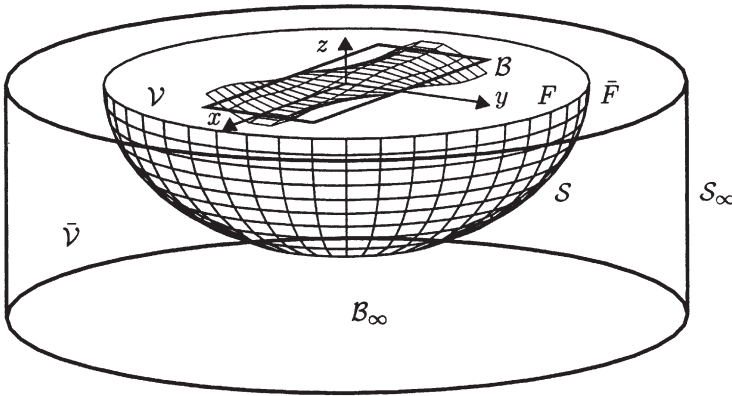Fig. 2.   Hydrodynamic coefficients for a floating disk.

Fig. 3.   Discretization for variational formulation.

conditions Eq. (24) satisfied as natural boundary conditions. This presupposes that the function $\tilde{\phi}_\alpha$ is selected from among those satisfying (i), (ii), the bottom condition, and the radiation condition, exactly. Noting that $\tilde{\phi}_\alpha \in V$ is bounded, including at the origin, it is proposed that it be expanded in spherical harmonics as

$$\tilde{\phi}_\alpha(\mathbf{r}) = \sum_{m=0}^{M} \sum_{n=0}^{N} A_{nm} \phi_{nm}(\mathbf{r}) + \sum_{m=1}^{M} \sum_{n=0}^{N} B_{nm} \psi_{nm}(\mathbf{r}) \tag{26}$$

where

$$\phi_{nm}(\mathbf{r}) = \left(\frac{R}{a_h}\right)^n P_n^m(\cos\theta)\cos m\psi, \quad \psi_{nm}(\mathbf{r}) = \left(\frac{R}{a_h}\right)^n P_n^m(\cos\theta)\sin m\psi. \tag{27}$$

Here $\{R, \theta, \psi\}$ are spherical coordinates such that

$$x = R\sin\theta\cos\psi, \ \ y = R\sin\theta\sin\psi, \ \ z = -R\cos\theta$$

and P_n^m are the associated Legendre Functions as defined by Hulme (1982).

Although not necessary here, each basis function satisfies Laplace's equation and is eminently suited to the hemispherical geometry.

It is proposed to express $\bar{\phi}_\alpha$ using a source distribution on S:

$$\bar{\phi}_\alpha(\mathbf{r}) = \int_S G(\mathbf{r},\boldsymbol{\xi})\gamma_\alpha(\boldsymbol{\xi})dS_\xi \tag{28}$$

where the source distribution $\gamma_\alpha(\mathbf{r})$ is selected according to

$$\frac{\partial\bar{\phi}_\alpha(\mathbf{r})}{\partial n} = -2\pi\gamma_\alpha(\mathbf{r}) + \int_S \frac{\partial G(\mathbf{r},\boldsymbol{\xi})}{\partial n_r}\gamma_\alpha(\boldsymbol{\xi})dS_\xi. \tag{29}$$

In practice, S is divided into a number of regions S_i and $\gamma_\alpha(\mathbf{r})$ is taken to be constant on each S_i with $\gamma_{\alpha,i} = \gamma_\alpha(\mathbf{r}_i)$ where $\mathbf{r}_i$ is the centrepoint of S_i. Defining $\bar{\mathbf{\Phi}}_\alpha$ $= \text{col}\{\bar{\phi}_{\alpha,i}\}$, $\bar{\mathbf{\Phi}}_{\alpha,n} = \text{col}\{\bar{\phi}_{\alpha n,i}\}$, $\bar{\phi}_{\alpha,i} = \bar{\phi}_\alpha(\mathbf{r}_i)$, $\bar{\phi}_{\alpha n,i} = \partial\bar{\phi}_{\alpha,i}(\mathbf{r}_i)/\partial n$ and $\mathbf{\gamma}_\alpha = \text{col}\{\gamma_{\alpha,i}\}$, Eqs. (13) and (14) can be approximated by

$$\mathbf{\Phi}_\alpha = \mathbf{G}\mathbf{\gamma}_\alpha, \mathbf{\Phi}_{\alpha,n} = \mathbf{H}\mathbf{\gamma}_\alpha \tag{30}$$

where

$$G_{ij} = G(\mathbf{r}_i, \mathbf{r}_j)\Delta S_j, \tag{31}$$

$$H_{ij} = -2\pi\delta_{ij} + \frac{\partial G(\mathbf{r}_i, \mathbf{r}_j)}{\partial n_r}\Delta S_j, \tag{32}$$

and $\Delta S_i = \int_{S_i} dS$.

Expanding $\tilde{\phi}_\alpha$ according to Eq. (26) and $\bar{\phi}_\alpha$ using Eq. (28) and the above discretization procedure, Eq. (25) becomes

$$J(\tilde{\phi}_\alpha, \bar{\phi}_\alpha) = J(\mathbf{b}_\alpha) = \frac{1}{2}\mathbf{b}_\alpha^T\mathbf{W}\mathbf{b}_\alpha - \mathbf{b}_\alpha^T\mathbf{c}_\alpha \tag{33}$$

where

$$\mathbf{b}_\alpha = \begin{bmatrix} \mathbf{a}_\alpha \\ \mathbf{\gamma}_\alpha \end{bmatrix}, \quad \mathbf{a}_\alpha = \begin{bmatrix} col\{A_{nm}\} \\ col\{B_{nm}\} \end{bmatrix}, \quad \mathbf{c}_\alpha = \begin{bmatrix} -\mathbf{g}_\alpha \\ 0 \end{bmatrix}, \quad \mathbf{g}_\alpha = \begin{bmatrix} col\{g_{\phi nm}\} \\ col\{g_{\psi nm}\} \end{bmatrix} \tag{34}$$

with

$$\begin{Bmatrix} g_{\phi,nm} \\ g_{\psi,nm} \end{Bmatrix} = P_n^m(0) \int_B (R/a_h)^n \begin{Bmatrix} cosm\psi \\ \sin m\psi \end{Bmatrix} n_\alpha(x,y)dA. \tag{35}$$

The matrix $\mathbf{W}$ is defined by

$$\mathbf{W} = \begin{bmatrix} \mathbf{K}_v - k\mathbf{K}_f & \mathbf{\Psi}^T\mathbf{H} \\ \mathbf{H}^T\mathbf{\Psi}^T & \frac{1}{2}(\mathbf{G}^T\mathbf{S}\mathbf{H} + \mathbf{H}^T\mathbf{S}\mathbf{G}) \end{bmatrix} = \mathbf{W}^T \tag{36}$$

where the various submatrices are given by

$$\mathbf{S} = diag\left\{\int_{S_i} dA\right\}, \quad \mathbf{\Psi} = row_i\begin{bmatrix} col\{\phi_{nm}(\mathbf{r}_i)\} \\ col\{\psi_{nm}(\mathbf{r}_i)\} \end{bmatrix}; \tag{37}$$

The matrix $\mathbf{K}_v$ is readily constructed integrals of the form

$$\int_V \nabla\phi_{nm}\cdot\nabla\phi_{lm}dV=\int_V \nabla\psi_{nm}\cdot\nabla\psi_{lm}dV=\frac{2\pi a_h}{\varepsilon_m(n+l+1)}J(n,l;m) \tag{38}$$

where $\varepsilon_m=1$, $m=0$, $\varepsilon_m=2$, $m=1,2,3,\dots$, is the Jacobi symbol, and

$$J(n,l;m)=\int_0^1\left[m^2\frac{P_l^m(x)P_n^m(x)}{1-x^2}+(1-x^2)\frac{dP_l^m(x)}{dx}\frac{dP_n^m(x)}{dx}+nlP_l^m(x)P_n^m(x)\right]dx \tag{39}$$

$$=\begin{cases}\frac{1}{n-l}\left[lP_l^m(0)\frac{dP_n^m(0)}{dx}-nP_n^m(0)\frac{dP_l^m(0)}{dx}\right], & n\neq l\\[2mm] \frac{1}{2n+1}\frac{(n+m)!}{(n-m)!}, & n=l\end{cases}$$

We note that although the $\nabla\phi_{nm}$ are orthogonal on the sphere, they are not on the hemisphere. The calculation for $J(n,l;m)$ follows from a derivation very similar to that in Appendix B of Hulme (1982).

The entries in $\mathbf{K}_f$ are readily constructed from integrals of the form

$$\int_F \phi_{nm}\phi_{lk}dA=\frac{2\pi a_h^2}{\varepsilon_m(n+l+2)}P_n^m(0)P_l^m(0)\delta_{\ln}-P_n^m(0)P_l^k(0)\int_B r^{n+l}\cos m\phi\,\cos k\phi dA \tag{40}$$

Minimizing J in Eq. (33) with respect to $\mathbf{b}_\alpha$ leads to a linear system of equations $\mathbf{W}\mathbf{b}_\alpha=\mathbf{c}_\alpha$ which can be solved for $\{\mathbf{a}_\alpha,\boldsymbol{\gamma}_\alpha\}$. The added mass and damping coeffients can then be calculated using $\tilde{H}_{R,\alpha\beta}(j\omega)=j\omega\rho\mathbf{g}_\beta{}^T\mathbf{a}_\alpha$ which follows from substituting Eq. (26) into Eq. (19).

4.2. Irregular frequencies

It is well known that the source distribution technique gives rise to the problem of irregular frequencies and its use in the variational method here is no exception. An effective way of dealing with the problem is to augment the Green's function with additional terms which continue to satisfy the boundary value problem and do not alter the source-like character at $\mathbf{r}=\boldsymbol{\xi}$. Motivated by the work of Ursell (1981), $G(\mathbf{r},\boldsymbol{\xi})$ in Eqs. (28) and (29) is replaced by

$$\hat{G}(\mathbf{r},\boldsymbol{\xi})=G(\mathbf{r},\boldsymbol{\xi})+\sum_{i=1}^{N_s}\alpha_i\left[G(\mathbf{r},\mathbf{r}_i)G(\boldsymbol{\xi},\mathbf{r}_i)+\frac{\partial G(\mathbf{r},\mathbf{r}_i)}{\partial x}\frac{\partial G(\boldsymbol{\xi},\mathbf{r}_i)}{\partial\xi}+\frac{\partial G(\mathbf{r},\mathbf{r}_i)}{\partial y}\frac{\partial G(\boldsymbol{\xi},\mathbf{r}_i)}{\partial\eta}\right]$$

$$+\sum_{m=0}^{M_p}\sum_{n=m+1}^{N_p}\beta_{nm}g_n^{2m}(\mathbf{r})g_n^{2m}(\boldsymbol{\xi}) \tag{41}$$

where

$$g_n^{2m}(\mathbf{r})=\left[\frac{k}{2(n-m)}\frac{1}{R^{2n}}P_{2n-1}^{2m}(\cos\theta)+\frac{1}{R^{2n+1}}P_{2n}^{2m}(\cos\theta)\right]\cos(2m\psi)$$

are even wave-free multipoles.

4.3. Diffraction problem

It has been demonstrated by Yue et al. (1978) that the solution of the diffraction problem $\tilde{\phi}_D\triangleq\tilde{\phi}_S+\tilde{\phi}_I$ can be determined by rendering the following functional stationary:

$$J_D(\tilde{\phi}_D,\bar{\phi}_S)=\frac{1}{2}\int_V\nabla\tilde{\phi}_D\cdot\nabla\tilde{\phi}_D dV-\frac{1}{2}k\int_F\tilde{\phi}_D^2 dS+\int_S\left(\frac{1}{2}\bar{\phi}_S-\tilde{\phi}_D\right)\frac{\partial\bar{\phi}_S}{\partial n}dS+\int_S\left(\tilde{\phi}_I\frac{\partial\bar{\phi}_S}{\partial n}\right.$$

$$\left.-\tilde{\phi}_D\frac{\partial\tilde{\phi}_I}{\partial n}\right)dS \tag{42}$$

This yields a function $\tilde{\phi}_D$ which satisfies Laplace's equation weakly in V with the free-suface condition on F, $\partial\tilde{\phi}_D/\partial n=0$ on B, and the matching conditions $\tilde{\phi}_D=\bar{\phi}_S+\tilde{\phi}_I$, $\tilde{\phi}_{D,n}=\bar{\phi}_{S,n}+\tilde{\phi}_{I,n}$ on S satisfied as natural boundary conditions.

The diffraction potential, $\tilde{\phi}_D$, can be expanded as in Eq. (26) (with $\mathbf{a}_\alpha$ replaced with $\mathbf{a}_D$) and $\bar{\phi}_S$ is expressed according to Eqs. (28) and (29) (with $\boldsymbol{\gamma}_\alpha$ replaced with $\boldsymbol{\gamma}_D$). Introducing these expansions into Eq. (42) leads to

$$J_D(\tilde{\phi}_D,\bar{\phi}_S)=J_D(\mathbf{b}_S)=\frac{1}{2}\mathbf{b}_D^T\mathbf{W}\mathbf{b}_D-\mathbf{b}_D^T\mathbf{c}_D$$

where

$$\mathbf{b}_D=\begin{bmatrix}\mathbf{a}_D\\\boldsymbol{\gamma}_D\end{bmatrix},\ c_D=\begin{bmatrix}\boldsymbol{\Psi}^T\mathbf{S}\boldsymbol{\Phi}_{In}\\-\mathbf{H}^T\mathbf{S}\boldsymbol{\Phi}_I\end{bmatrix},$$

$\boldsymbol{\Phi}_I=\mathrm{col}\{\tilde{\phi}_I(\mathbf{r}_i)\}$, and $\boldsymbol{\Phi}_{In}=\mathrm{col}\{\tilde{\phi}_{I,n}(\mathbf{r}_i)\}$. Minimization of this quadratic form leads to a linear system of equation for $\{\mathbf{a}_D,\boldsymbol{\gamma}_D\}$ which can be used to form $\tilde{H}_{D\alpha}$ $(j\omega)=j\omega\rho\mathbf{g}_\alpha^T\mathbf{a}_D$.

4.4. Haskind relations

A useful check on the accuracy of the above procedures is provided by the Haskind relations which allow $\tilde{H}_{D\alpha}$ to be solved using the solution $\tilde{\phi}_\alpha$ of the radiation problem:

$$\tilde{H}_{D\alpha}(j\omega) = j\omega\rho\int_B [\tilde{\phi}_I\tilde{\phi}_{\alpha,n} - \tilde{\phi}_\alpha\tilde{\phi}_{I,n}]dA$$

$$= j\omega\rho\int_S [\tilde{\phi}_I\tilde{\phi}_{\alpha,n} - \tilde{\phi}_\alpha\tilde{\phi}_{I,n}]dS \tag{43}$$

$$= j\omega\rho[\mathbf{\Phi}_I^T\mathbf{SH} - \mathbf{\Phi}_{I,n}^T\mathbf{SG}]\gamma_\alpha,$$

where Green's formula has been used to convert the surface integral over the plate to a surface integral over the hemisphere. Not only is the radiation potential used in lieu of solving for the scattered potential but the calculation uses its far-field representation in terms of the source distribution and is performed on the hemispherical interface.

4.5. Far-field calculation

From Mei, the far-field behaviour of the radiation potential can be written as

$$\bar{\phi}_\alpha = \frac{jg}{\omega}e^{kz}\sqrt{\frac{2}{\pi kr}}e^{-j(kr-\pi/r)}A_\alpha(\psi) \tag{44}$$

and $A_\alpha(\psi)$ can be calculated based on the values of $\bar{\phi}_\alpha$ and $\bar{\phi}_{\alpha,n}$ for $r\in S$:

$$A_\alpha(\psi) = -\frac{2\pi k^2}{\omega}\int_S \exp[jk(x\cos\psi+y\sin\psi)+kz]\gamma_\alpha(r)dS(r) \tag{45}$$

$$= -\frac{k^2}{2\omega}\int_S\left[\bar{\phi}_\alpha\mathbf{n}^T[jk\cos\psi \ \ jk\sin\psi \ \ k]^T - \frac{\partial\bar{\phi}_\alpha}{\partial n}\right]\times$$

$$\exp[jk(x\cos\psi+y\sin\psi)+kz]dS \tag{46}$$

This provides a useful check using the identity

$$\lambda_{\alpha\beta} = \frac{\rho g^3}{\pi\omega^3}\int_0^{2\pi} A_\alpha(\psi)A_\beta^*(\psi)d\psi \tag{47}$$

A calculation analogous to Eq. (46) using $\tilde{\phi}_S$ yields the far-field behavior, $A_s(\psi)$, of the scattered potential.

As noted by Mei (1989), the Kochin functions $A_\alpha(\psi)$ and $A_S(\psi)$ permit other important checks to be made using the following identities:

$$\tilde{H}_{D\alpha} = -\frac{2\rho g^3}{\omega^3} A_\alpha(\psi_I + \pi) \text{ (Haskind–Hanoako)} \tag{48}$$

$$A_\alpha(\psi_I + \pi) - A_\alpha^*(\psi_I) = \frac{1}{\pi} \int_0^{2\pi} A_\alpha^*(\psi) A_S(\psi) d\psi \text{ (Bessho–Newman relations)} \tag{49}$$

$$-Re\{A_S(\psi_I)\} = \frac{1}{2\pi} \int_0^{2\pi} |A_S(\psi)|^2 d\psi \text{ (Optical theorem)} \tag{50}$$

where $\psi_I = 0$ denotes the propagation direction of the incident wave.

4.6. Example — the heaving disc

This example affords us the opportunity to compare the variational technique with the integral equation method on a relatively simple dock problem with previously published results and known asymptotics. We consider the heaving motion of a circular disk with radius a. The enclosing hemisphere with radius $a_h = 5a/4$ is panelled with a 40 (circumferential)×12 (radial) array of panels with dimensions $\Delta\psi = 2\pi/40$ and $\Delta\theta = \pi/12$. In the interior expansion in Eq. (26), $M = 18$ and $N = 10$ which leads to a total (including the source panels) of 901 degrees of freedom. The augmentation of the Green's function in Eq. (41) is accomplished with a single source and dipole combination ($N_s = 1$, $\alpha_1 = 1 + j$) and and a single wave-free potential ($M_p = 0$, $N_p = 1$, $\beta_{0,0} = 1 + j$). The integrals in Eqs. (35) and (40) can be done analytically for this case.

The resulting added mass and damping coefficients along with the heave force coefficients are shown in Fig. 2 along with those obtained using the panel method. The added mass and damping coefficients are in excellent agreement with those provided by Miles (1987). The behavior of the panel method at "high" frequencies ($ka > 1$) is consistent with the observations of Buchner (1993); the added mass and damping is underestimated with the former tending towards zero as opposed to the correct nonzero value. The force coefficients calculated using the variational and panel methods are in reasonable agreement with the former being presumably more accurate. The force coefficients calculated using the Haskind relations in Eq. (43) typically agreed with the "variational" curves to within 0.1% at all frequencies.

5. Numerical study of the hydrodynamic coefficients

We now consider a rectangular plate with dimensions $a \times b$ with $a/b = 2.5$. The use of a 10×10 array of Legendre polynomials for spatial discretization produced the first ten modes and frequencies shown in Fig. 4. Notice that all modes exhibit either symmetry or antisymmetry about the x- and y-axes. The enclosing hemisphere in Fig. 3 was chosen to be circumscribing with radius $a_h = \sqrt{a^2 + b^2}/4$. The arrangement of sources on the hemisphere and the number of spherical harmonics used in its
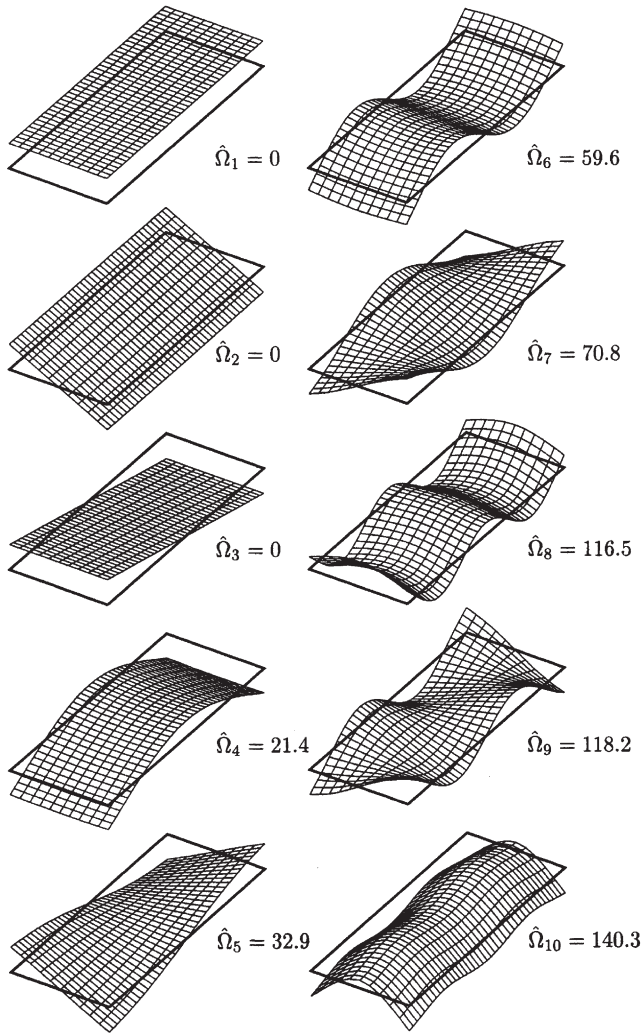
Fig. 4.   Plate vibration modes $[\Omega^2_\alpha = D/(\sigma a^4)\ \hat{\Omega}^2_\alpha]$.

interior was identical to that used in the last section for the disc. It was found that by choosing N_s=13 in Eq. (41) with a source and dipole combination at the origin and the remaining 12 located at $(x,y,z)=(\pm a/2, \pm b/2, 0)$, $(\pm a/2, 0, 0)$, $(0, \pm b/2, 0)$, $(\pm a/4, \pm b/4, 0)$, M_p=1, N_p=2, and $\alpha_i = \beta_{nm} \equiv 0.1/(ka)$, irregular frequencies in the interval $0 \leq ka \leq 20$ could be suppressed.

The resulting added mass and damping coefficients are shown in Figs. 5 and 6. Also shown are the resulting curves using a panel method with a 40×16 grid of identical rectangular panels on the plate. The agreement between the two methods is better here than it was for the disc. Once again, the panel method underestimates
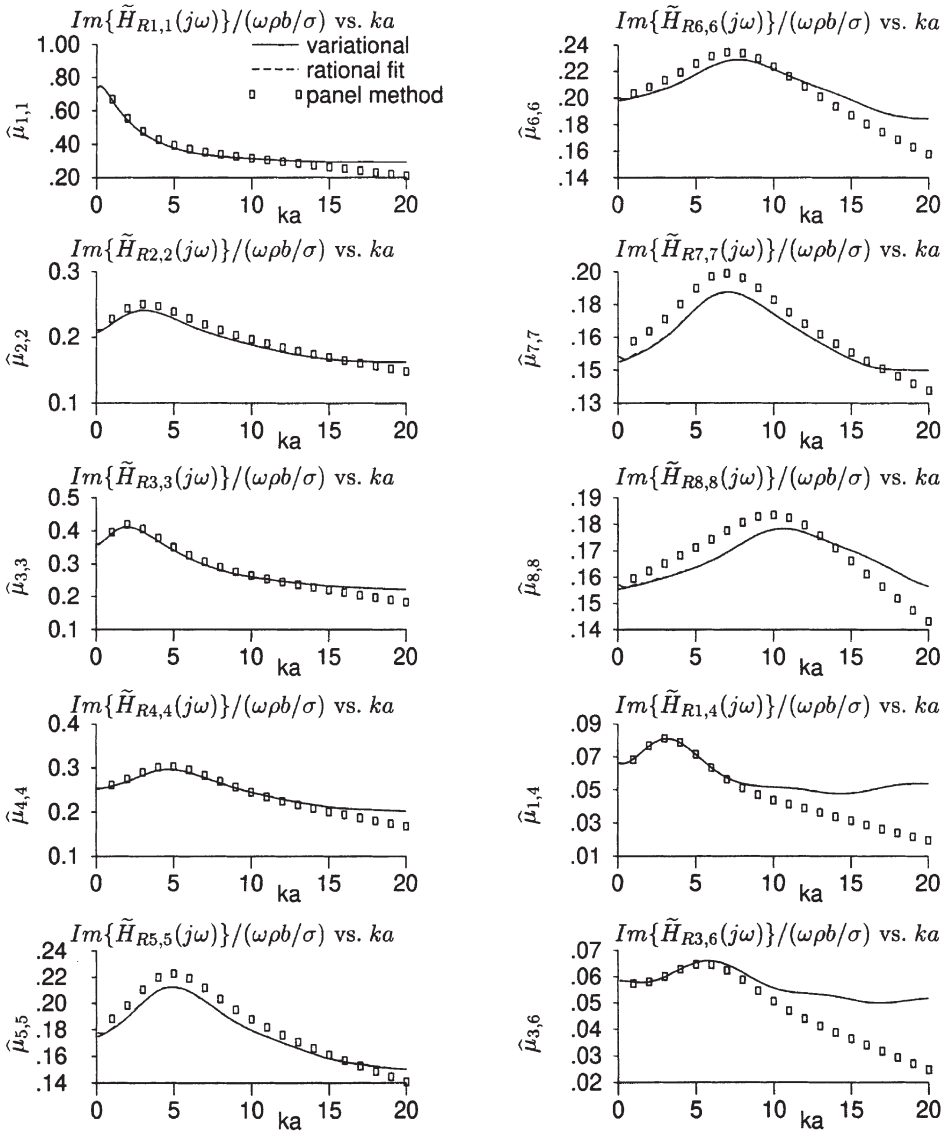
Fig. 5.   Added mass coefficients for a plate [$\hat{\mu}_{\alpha\beta} = \mu_{\alpha\beta}/(\rho b/\sigma)$].

the added damping at high frequency. It should be noted that the only nonzero off-diagonal added mass coefficients for $1 \leq \alpha, \beta \leq 8$ are $\mu_{1,4}$, $\mu_{1,8}$, $\mu_{2,7}$, $\mu_{3,6}$, and $\mu_{4,8}$ with a similar comment for the added damping coefficients. These correspond to mode pairs that exhibit the identical symmetries about the x- and y-axes. Only the cases $\mu_{1,4}$ ($\lambda_{1,4}$) and $\mu_{3,6}$ ($\lambda_{3,6}$) are shown on account of space limitations. The curves labelled "rational fit" will be discussed in the next section.
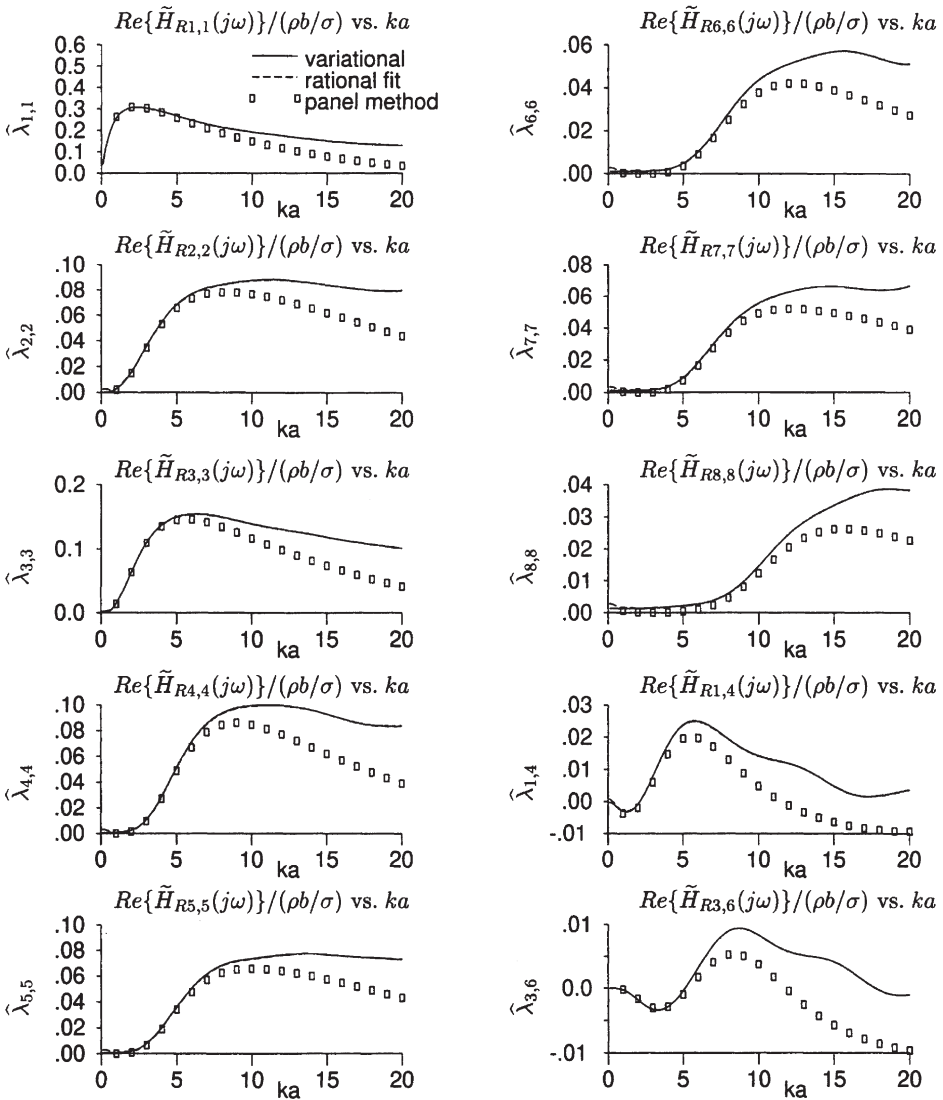
Fig. 6.   Added damping coefficients for a plate $[\hat{\lambda}_{\alpha\beta}=\lambda_{\alpha\beta}/(\rho b/\sigma)]$.

The only nonzero diffraction force coefficients correspond to α=1,3,4,6,8 which are modes exhibiting even symmetry about the x-axis. The real and imaginary parts are shown in Fig. 7 along with those obtained using the Haskind relations. There is no graphical difference between the two. The far-field patterns $A_S(\psi)$ and $A_\alpha(\psi)$, α=1,…,8 were determined using Eq. (46) and are shown in Fig. 8 for ka=1 and Fig. 9 for ka=10. The identities presented in Eqs. (48)–(50) were tested numerically; it is readily verified that the Haskind–Hanoako identity in Eq. (48) in conjunction with
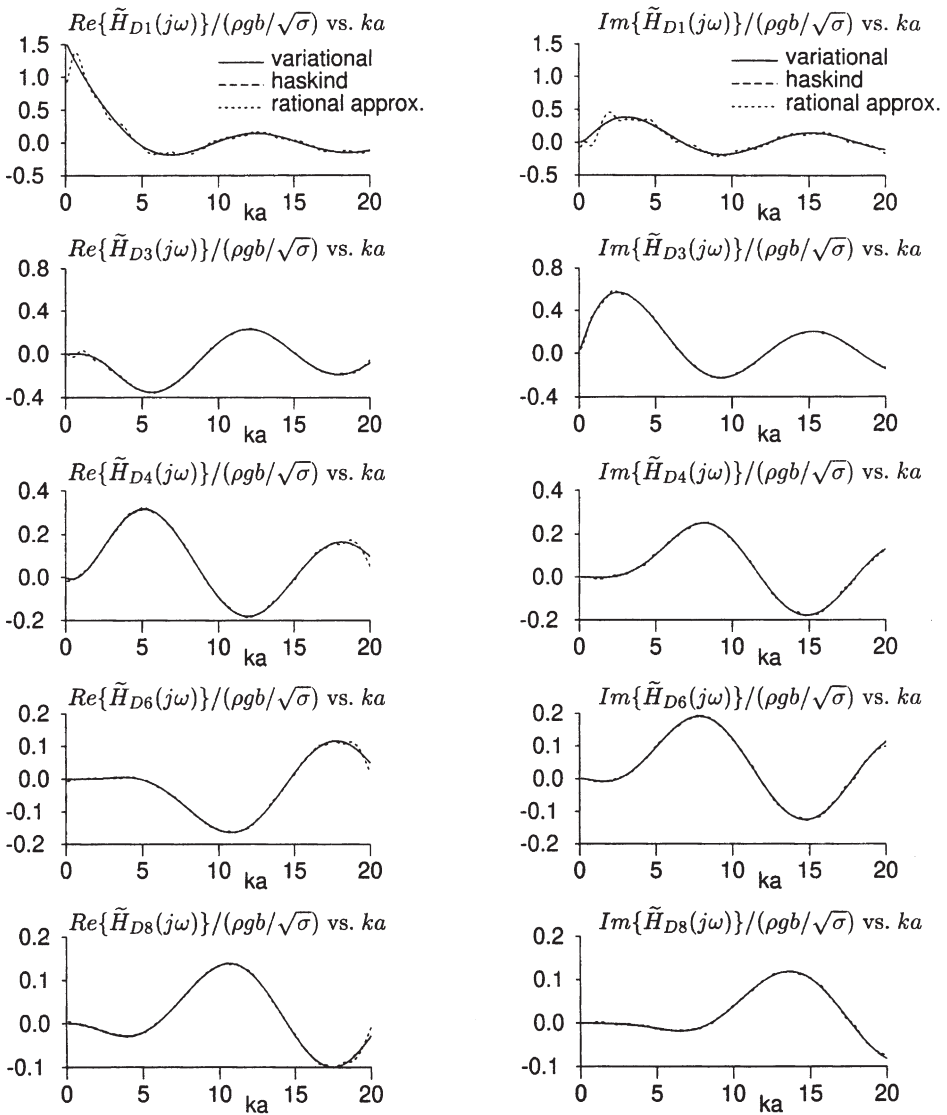
Fig. 7.   Generalized diffraction force coefficients.

Eq. (46) is equivalent to the Haskind relations. For ka=1, the left-hand and right-hand sides of Eq. (50), respectively, were 0.378 and 0.388, and for ka=10, 5.42 and 5.28. The results of evaluating the left- and right-hand sides of Eq. (47) appear in Table 1. Similar agreement was exhibited by the Bessho–Newman relations in Eq. (49).
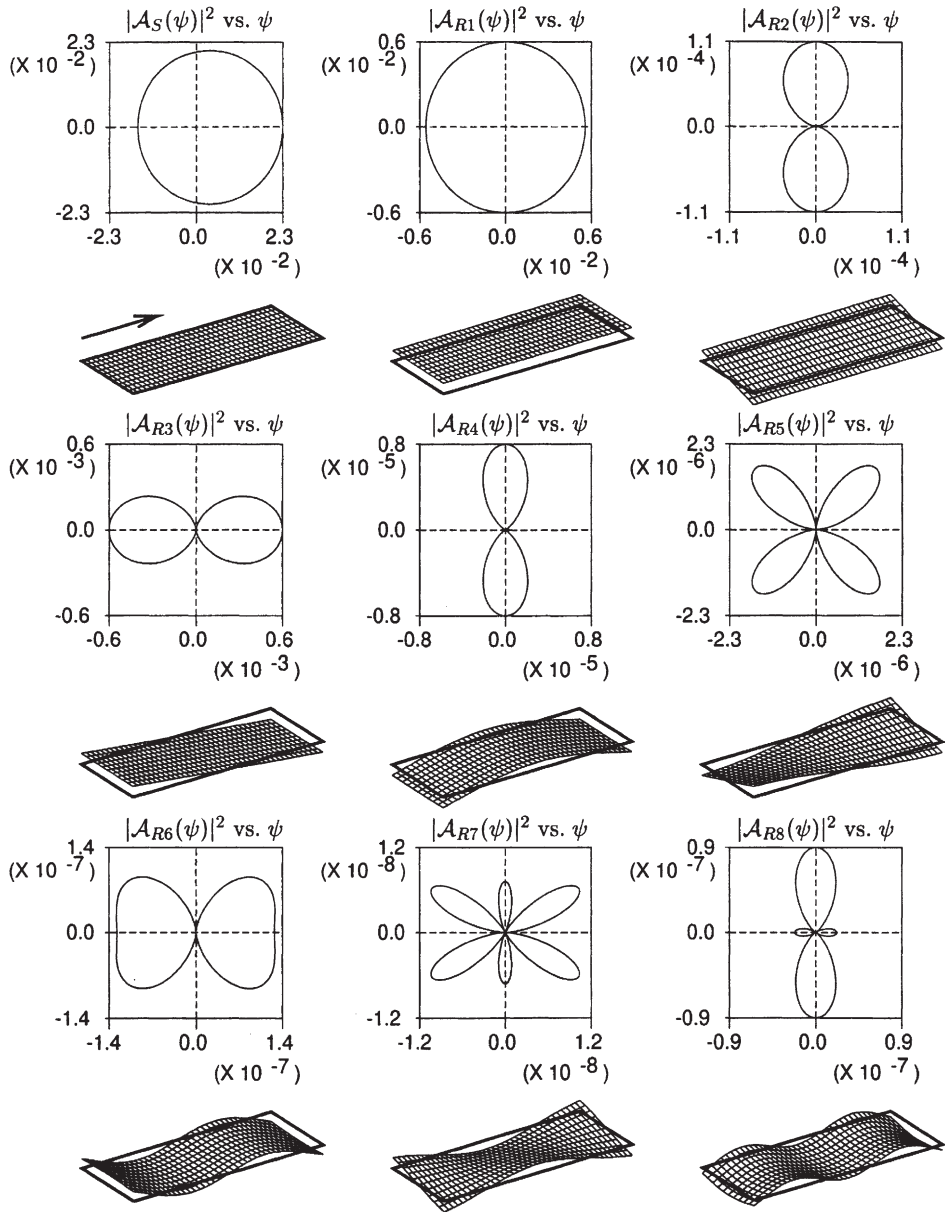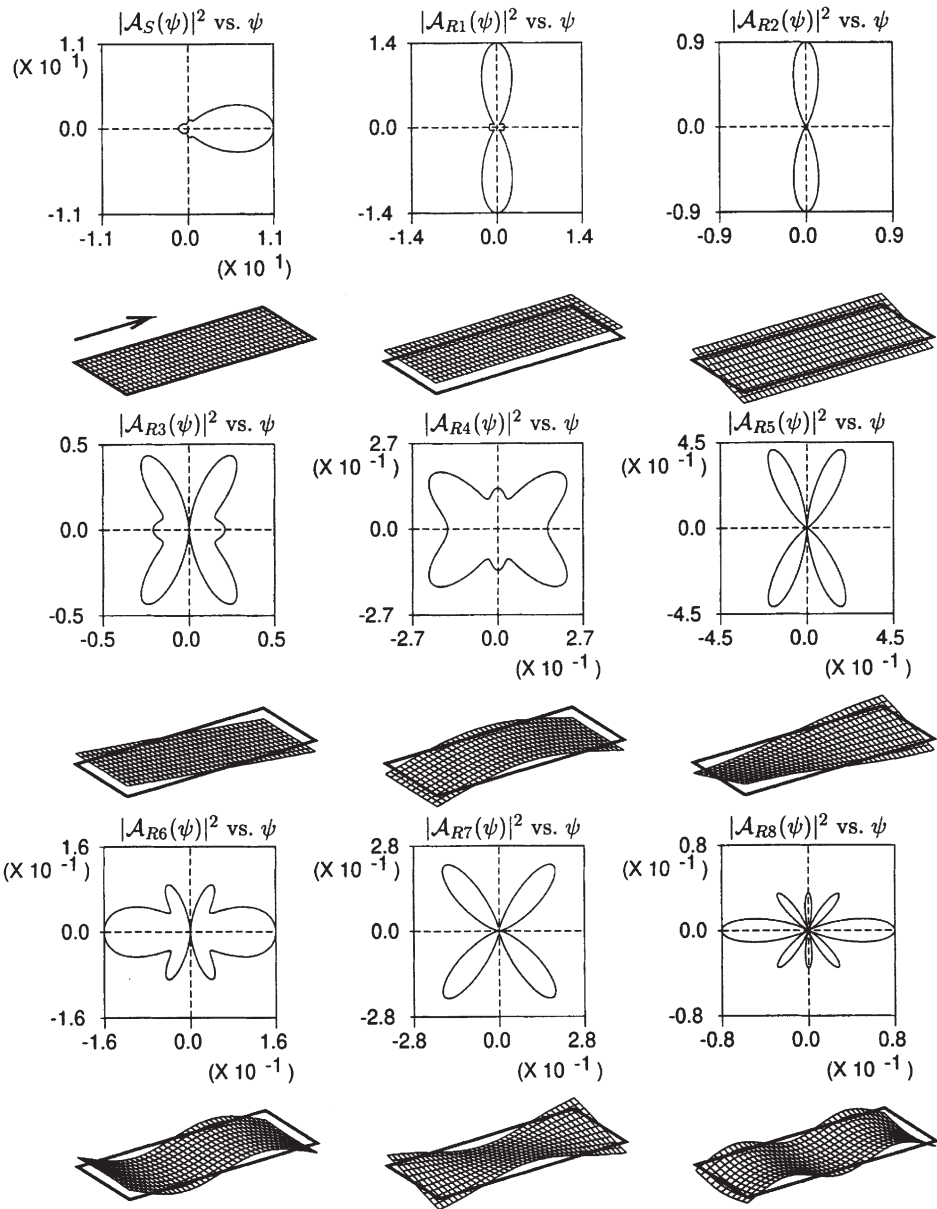
Fig. 8.   Far-field patterns (ka=1).

Fig. 9.   Far-field patterns (ka=10).

6. Transient formulation

In this section, the frequency domain information acquired in the last section will be used to realize the overall mapping from incident wave height $\zeta_0(t)$ to plate motion

Table 1
Identities involving far-field potentials

	$ka=1$ Eq. (47)		$ka=10$ Eq. (47)	
α	LHS	RHS	LHS	RHS
1	0.259	0.262	0.193	0.187
2	2.68×10^{-3}	2.69×10^{-3}	0.0853	0.0826
3	0.01419	0.01420	0.138	0.134
4	1.3×10^{-4}	7.3×10^{-5}	0.0912	0.0883
5	4.4×10^{-5}	5.8×10^{-5}	0.0714	0.0692
6	-2.9×10^{-6}	4.9×10^{-6}	0.0431	0.0418
7	-1.1×10^{-5}	2.5×10^{-7}	0.0537	0.0519
8	-4.9×10^{-7}	1.5×10^{-6}	0.0137	0.0132

$w(x_i,y_i,t)$ as a system of constant–coefficient ordinary differential equations (ODE's). This will be accomplished by fitting the Fourier transforms of the impulse responses of the radiation impedance and diffraction mappings with rational functions of the Laplace transform variable s.

It is assumed that N_e modes contribute to the expansion for $w(x_i,y_i,t)$. Defining $\boldsymbol{\eta}(t)=\text{col}\{\eta_\alpha\}$, $\boldsymbol{\Omega}=\text{diag}\{\Omega_\alpha\}$, $\mathbf{f}_R(t)=\text{col}\{f_{R\alpha}\}$, $\mathbf{f}_D(t)=\text{col}\{f_{D\alpha}\}$, $\mathbf{C}_w=\text{row}\{w_\alpha(x_i,y_i)\}$, $\alpha=1,\ldots,N_e$ with $\mathbf{K}_s=\text{matrix}\{K_{s,\alpha\beta}\}$, Eq. (4) coupled with the time-domain version of Eq. (15) yields

$$w(x_i,y_i,t)=\mathbf{C}_w\boldsymbol{\eta}(t),\ddot{\boldsymbol{\eta}}+(\boldsymbol{\Omega}^2+\mathbf{K}_s)\boldsymbol{\eta}=\mathbf{f}_D(t)+\mathbf{f}_R(t) \tag{51}$$

Defining $\tilde{\mathbf{H}}_D(s)=\text{col}\{\tilde{\mathbf{H}}_{D\alpha}(s)\}$, $\tilde{\mathbf{H}}_R(s)=\text{matrix}\{\tilde{H}_{R,\alpha\beta}(s)\}$, then

$$\tilde{\mathbf{f}}_D(s)=\tilde{\mathbf{H}}_D(s)\tilde{\zeta}_0(s) \tag{52}$$

$$\tilde{\mathbf{f}}_R(s)=\tilde{\mathbf{H}}_R(s)\tilde{\boldsymbol{\eta}}(s) \tag{53}$$

Typically, $\tilde{H}_D(s)$ is noncausal as discussed by Falnes (1995) and has poles in $\text{Re}\{s\}>0$. It can be rendered approximately causal by writing Eq. (16) as

$$\tilde{f}_{D\alpha}(j\omega)=[\tilde{H}_{D\alpha}(j\omega)e^{-jk'x_I}][e^{jk'x_I}\tilde{\zeta}_0(j\omega)] \tag{54}$$

The term on the far right is the Fourier transform of the incident wave height at $x=x_I$, $\zeta_I(x_I,y,t)$. Numerical experience indicates that setting $x_I=-2a$ has the effect of rendering $\tilde{X}_\alpha(j\omega)=\tilde{H}_{D\alpha}(j\omega)e^{-jk'x_I}$ close to causal. Following the procedures of Damaren (1999), the corresponding s-domain mapping is approximated by

$$\tilde{X}_\alpha(s)=\frac{b_{D\alpha}(s)}{a_D(s)}=\frac{\displaystyle\sum_{i=1}^{n}b_{\alpha i}s^{n-i}}{s^n+\displaystyle\sum_{i=1}^{n}a_{di}s^{n-i}} \tag{55}$$

where $b_{\alpha i}$, a_{di}, $i=1\dots n$, are designed to fit the values of $\tilde{H}_{D\alpha}(j\omega)e^{-jk'x_I}$ obtained in the last section. It is desired that $a_D(s)$ have poles in $\text{Re}\{s\}<0$ and the same denominator polynomial is used for each $\tilde{X}_\alpha(s)$. Initially n was set to 10 and and individual rational fits of the form $b_{D\alpha}(s)/a_{D\alpha}(s)$ were developed for the nontrivial cases $\alpha=1,3,4,6,$ and 8. A denominator $a_D(s)$ of 50th degree was then formed as the product of the individual $a_{D\alpha}(s)$ and the $b_{\alpha i}$ were then obtained using a final least-squares fit. The fitted functions $\tilde{X}_\alpha(j\omega)e^{jk'x_I}$ are also shown in Fig. 7 for $x_I=-2a$.

The use of Eq. (55) for $\tilde{X}_\alpha(j\omega)$ in Eq. (54) followed by inverse Fourier transformation permits the transient diffraction mapping to be realized as

$$\mathbf{f}_D(t)=\mathbf{C}_d\mathbf{x}_d,\ \dot{\mathbf{x}}_d=\mathbf{A}_d\mathbf{x}_d+\mathbf{B}_d\zeta_I(-2a,y,t) \tag{56}$$

where

$$\mathbf{C}_d=\text{matrix}\{b_{\alpha i}\},\ \mathbf{A}_d=\begin{bmatrix} -a_{d1} & -a_{d2} & \dots & a_{d,n-1} & -a_{dn} \\ 1 & 0 & \dots & 0 & 0 \\ 0 & 1 & \dots & 0 & 0 \\ \vdots & \vdots & \ddots & \vdots & \vdots \\ 0 & 0 & \dots & 1 & 0 \end{bmatrix},\ \mathbf{B}_d=\begin{bmatrix} 1 \\ 0 \\ 0 \\ \vdots \\ 0 \end{bmatrix},$$

with $\mathbf{x}_D=0$.

The radiation impedance can be further written as

$$\tilde{\mathbf{H}}_R(s)=\tilde{\mathbf{H}}_r(s)+s\mathbf{M}_\infty,\ \mathbf{M}_\infty=\text{matrix}\{\lim_{\omega\to\infty}\mu_{\alpha\beta}\}. \tag{57}$$

The high frequency asymptote of the added mass coefficient can be calculated using the following relation due to Greenhow (1984):

$$\lim_{ka\to\infty}\mu_{\alpha\beta}(ka)=\frac{1}{2}\mu_{\alpha\beta}(Ka)+\frac{1}{4\sqrt{Ka}}\int_0^{Ka}\frac{\mu_{\alpha\beta}(z)}{\sqrt{z}}\,dz+O[(Ka)^{-2}]$$

and is used here with $Ka=20$ and 200 values of $\mu_{\alpha\beta}(ka)$ for $0\le ka\le20$ are used to approximate the integral. Again, following Damaren (1999) the properties of $H_r(s)$ (it is a positive real matrix function of s) suggests the following rational approximation:

$$\hat{\mathbf{H}}_r(s)=\sum_{k=1}^{n'}\mathbf{W}_{Rk}\frac{s}{s^2+2\zeta_{Rk}\Omega_{Rk}s+\Omega_{Rk}^2},\ \zeta_{Rk}>0,\ \Omega_{Rk}>0,\ \mathbf{W}_{Rk}=\mathbf{W}_{Rk}^T \tag{58}$$

where $\mathbf{W}_{Rk}$, ζ_{Rk}, and Ω_{Rk} are selected so that $\hat{\mathbf{H}}_r(j\omega)$ fits the values of $\tilde{H}_{r,\alpha\beta}(j\omega)=\lambda_{\alpha\beta}(j\omega)+j\omega[\mu_{\alpha\beta}(j\omega)-\mu_{\alpha\beta}(\infty)]$. The values of ζ_{Rk} and Ω_{Rk} are determined by finding functions of the form of Eq. (55) to fit the diagonal terms $\tilde{H}_{r,\alpha\alpha}(s)$. With these parameters then fixed, the quantities $W_{Rk,\alpha\alpha}$ are determined by approximating $\tilde{H}_{r,\alpha\beta}(j\omega)$ with fixed poles according to Eq. (58). Combining Eq. (53) with Eqs. (57) and (58) yields the following time-domain realization for the radiation impedance:

$$\mathbf{f}_R(t) = -\mathbf{M}_\infty \ddot{\boldsymbol{\eta}} + \mathbf{f}_r(t), \tag{59}$$

$$\mathbf{f}_r(t) = -\mathbf{W}_r \dot{\mathbf{q}}_r, \ \ddot{\mathbf{q}}_r + \mathbf{D}_r \dot{\mathbf{q}}_r + \mathbf{K}_r \mathbf{q}_r = \mathbf{B}_r \dot{\boldsymbol{\eta}} \tag{60}$$

where $\mathbf{B}_r = \mathrm{col}\{\mathbf{1}_{Ne}\}$, $\mathbf{W}_r = \mathrm{row}\{\mathbf{W}_{Rk}\}$, $\mathbf{D}_r = \mathrm{block}\ \mathrm{diag}\{2\zeta_{Rk}\Omega_{Rk}\mathbf{1}_{Ne}\}$, $\mathbf{K}_r = \mathrm{block}$ $\mathrm{diag}\{\Omega_k^2 \mathbf{1}_{Ne}\}$, and $\mathbf{1}_{Ne}$ is the $N_e \times N_e$ identity matrix. Hence, there are $N_e \times n'$ coordinates in $\mathbf{q}_r$.

The final transient state-space model can be obtained by combining the above results. Defining,

$$\mathbf{x}(t) = \begin{bmatrix} \boldsymbol{\eta} \\ (\mathbf{1}+\mathbf{M}_\infty)\dot{\boldsymbol{\eta}} \\ \mathbf{q}_r \\ \dot{\mathbf{q}}_r \\ \mathbf{x}_d \end{bmatrix}, \ \mathbf{A} = \begin{bmatrix} \mathbf{0} & (\mathbf{1}+\mathbf{M}_\infty)^{-1} & \mathbf{0} & \mathbf{0} & \mathbf{0} \\ -(\boldsymbol{\Omega}^2+\mathbf{K}_s) & \mathbf{0} & \mathbf{0} & -\mathbf{W}_R & \mathbf{C}_D \\ \mathbf{0} & \mathbf{0} & \mathbf{0} & \mathbf{1} & \mathbf{0} \\ \mathbf{0} & \mathbf{B}_r(\mathbf{1}+\mathbf{M}_\infty)^{-1} & -\mathbf{K}_r & -\mathbf{D}_r & \mathbf{0} \\ \mathbf{0} & \mathbf{0} & \mathbf{0} & \mathbf{0} & \mathbf{A}_D \end{bmatrix} \tag{61}$$

$$\mathbf{B}^T = [\mathbf{0}\ \ \mathbf{0}\ \ \mathbf{0}\ \ \mathbf{0}\ \ \mathbf{B}_D^T], \mathbf{C} = [\mathbf{C}_w\ \ \mathbf{0}\ \ \mathbf{0}\ \ \mathbf{0}\ \ \mathbf{0}]. \tag{62}$$

the model formed by combining Eqs. (51), (56) and (60) takes the form

$$y(t) = w(x_i, y_i, t) = \mathbf{C}\mathbf{x}(t), \ \dot{\mathbf{x}} = \mathbf{A}\mathbf{x} + \mathbf{B}\zeta_I(-2a, 0, t) \tag{63}$$

which is a time-domain realization of the composite system depicted in Fig. 1.

In an effort to demonstrate the utillity of this model, the response $y(t)$ to a time series for $\zeta_I(-2a, 0, t)$ constructed using a modified Pierson–Moskowitz spectrum with significant wave height $H_{1/3} = a$ and a mean wave period of $T_2 = \sqrt{[(a/g)]}$ is determined by integrating Eq. (63). The plate deflection is calculated at $(x_i, y_i) = (a/4, b/4)$ and it and the incident wave height are shown in Fig. 10 for the following parameters:

$$\frac{D}{\sigma g a^3} = 0.05, \ \frac{\rho a}{\sigma} = 10.$$

In addition to the effect of the incident wave field, it is easy to accomodate additional loads such as a moving point load emulating an aircraft landing. For example if $p(x, y, t)$ in Eq. (4) is augmented with a term of the form $f_\delta \delta(x - ct + a/2)$ with $c = a/T_\delta$, this effect can be captured by augmenting the right-hand side of the differential equation in Eq. (63) with a term of the form $\mathbf{d}_\delta(t) = \mathrm{col}\{\mathbf{0}, \mathrm{col}\{w_\alpha(ct - a/2, 0)\}, \mathbf{0}, \mathbf{0}, \mathbf{0}\}$. The resulting plate deflection for $T_\delta = 5\sqrt{[(a/g)]}$ and $f_\delta = \sigma g\ ab$ is also shown in Fig. 10.

7. Concluding remarks

The frequency domain hydrodynamics of a floating flexible plate have been considered using the Chen and Mei variational principle. The inner field was modeled using a spherical harmonic expansion which is consistent with the zero-draft nature of the thin-plate model and circumvented problems associated with distributing
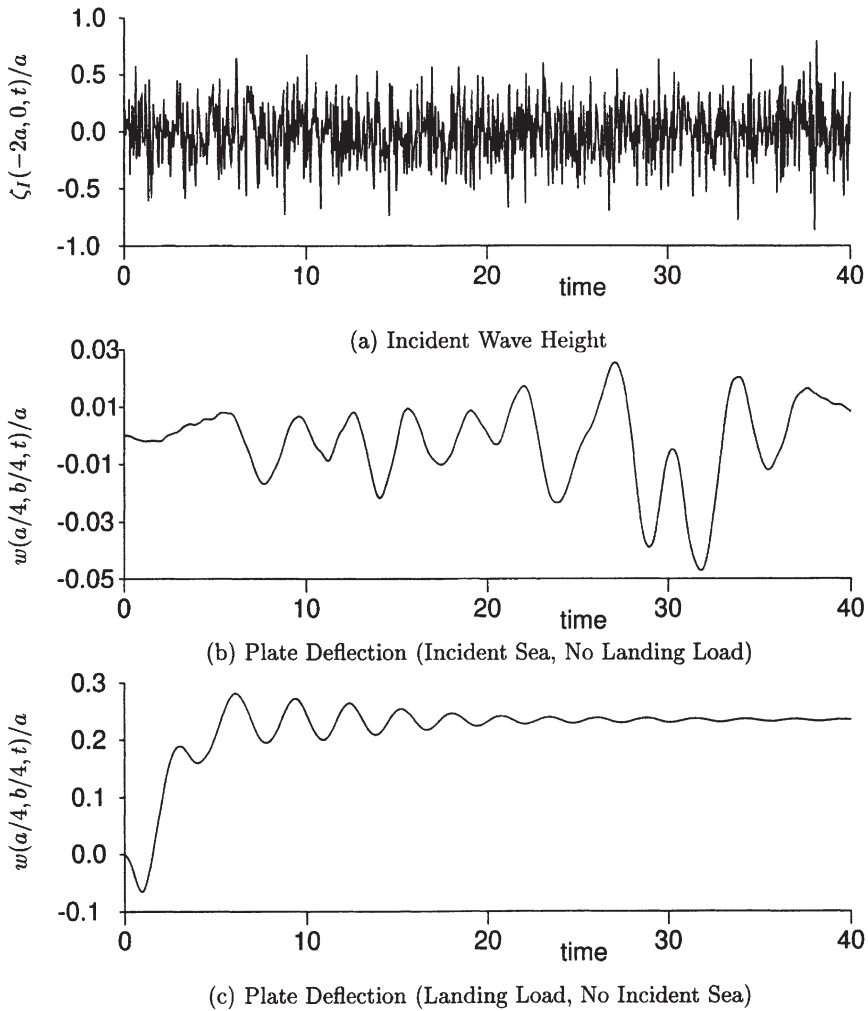
(a) Incident Wave Height

(b) Plate Deflection (Incident Sea, No Landing Load)

(c) Plate Deflection (Landing Load, No Incident Sea)

Fig. 10.   Transient wave height and plate deflection (time = $\sqrt{[g/a]}$).

sources in the free surface. The outer field was modeled using a source distribution on the boundary hemisphere which satisfies the far-field radiation condition and was matched to the inner field using the variational principle. The hydrodynamic coefficients presented here are seen as benchmark data for the analysis of flexible mat-like structures.

Contrary to previously published works, both the radiation and diffraction problems were considered here. The validity of the approach was established by comparing the results for a heaving disc with those obtained elsewhere. A transient model relating the incident sea state to the motion of the plate was created by using rational

approximations in the frequency domain which correspond to constant–coefficient ordinary differential equations in the time domain.

References

Buchner, B., 1993. An evaluation and extension of the shallow draft diffraction theory. Proc. of the Third International Offshore and Polar Engineering Conference, Singapore, pp. 230–241.

Chen, H.S., Mei, C.C., 1974. Oscillations and wave forces in a man-made harbor in the open sea. Tenth Symposium on Naval Research, Office of Naval Research, pp. 573–594.

Damaren, C.J., 1999. Time-domain floating body dynamics by rational approximation of the radiation impedance and diffraction mapping. Ocean Engineering 27, 687–705.

Falnes, J., 1995. On non-causal impulse response functions related to propagating water waves. Applied Ocean Research 17, 379–389.

Greenhow, M., 1984. A note on the high-frequency limits of a floating body. J. Ship Research 28, 226–228.

Hulme, A., 1982. The wave forces acting on a floating hemisphere undergoing forced periodic oscillations. J. Fluid Mechanics 121, 443–463.

Martin, P.A., Farina, L., 1997. Radiation of water waves by a heaving submerged horizontal disc. J. Fluid Mechanics 337, 365–379.

Mei, C.C., 1989. The Applied Dynamics of Ocean Surface Waves, 2nd ed. World Scientific, Singapore.

Meylan, M.H., 1997. The forced vibration of a thin plate floating on an infinite liquid. J. Sound and Vibration 205, 581–591.

Miles, J.W., 1987. On surface-wave forcing by a circular disk. J. Fluid Mechanics 175, 97–108.

Newman, J.N., 1984. Double-precision evaluation of the oscillatory source potential. J. Ship Research 28, 151–154.

Newman, J.N., 1994. Wave effects on deformable bodies. Applied Ocean Research 16, 47–59.

Ursell, F., 1981. Irregular frequencies and the motion of floating bodies. J. Fluid Mechanics 105, 143–156.

Wehausen, J.V., 1971. The motion of floating bodies. Annual Review of Fluid Mechanics 3, 237–268.

Wu, C., Watanabe, E., Utsunomiya, T., 1995. An eigenfunction expansion-matching method for analyzing the wave-induced responses of an elastic floating plate. Applied Ocean Research 17, 301–310.

Yue, D.K.P., Chen, H.S., Mei, C.C., 1978. A hybrid element method for diffraction of water waves by three-dimensional bodies. Int. J. Num. Meth. Eng. 12, 245–266.